Annealing process of ion-implantation-induced defects in ZnO: Chemical effect of the ion species

Z. Q. Chen[a)]
Department of Physics, Wuhan University, Wuhan 430072, People's Republic of China

M. Maekawa, A. Kawasuso, S. Sakai, and H. Naramoto
Advanced Science Research Center, Japan Atomic Energy Research Institute, 1233 Watanuki, Takasaki, Gunma 370-1292, Japan

(Received 26 November 2005; accepted 10 March 2006; published online 12 May 2006)

ZnO single crystals implanted with O^+ and B^+ ions were studied by positron annihilation and Raman scattering measurements. Positron annihilation results show that vacancy clusters are generated by implantation. For the B^+-implanted sample, the vacancy clusters have a sufficient increase in size and evolve into microvoids after annealing up to 500 °C. These microvoids need a high temperature of 900–1000 °C to be annealed out. However, for the O^+-implanted sample, the size of the vacancy clusters shows only a slight increase during annealing process, and they are removed at much lower temperature of 700–800 °C. The different annealing process is supposed to be due to the chemical effect of boron impurities. Raman measurements reveal the production of oxygen vacancies by implantation. In the B^+-implanted sample they have high thermal stability up to 700 °C, while in the O^+-implanted sample they are annealed out early at 400 °C. It is thus suggested that the boron impurities might form complexes with oxygen interstitials and stabilize oxygen vacancies, which favors the vacancy agglomeration process. © *2006 American Institute of Physics*.
[DOI: 10.1063/1.2194113]

I. INTRODUCTION

Ion implantation for the purpose of doping and isolation has become an indispensable processing tool for the production of semiconductor devices. It is a convenient method to incorporate dopants into semiconductor materials with precisely controllable amounts in a much shorter time. The other advantages lie in that the dopants can be incorporated independent of the solubility, and the doping area can also be selected. However, one main disadvantage of this method is the severe radiation damage, which strongly affects the electrical and optical properties and cause unexpected degradation effects of the devices. Therefore, a postimplantation annealing to remove the implantation-induced defects is necessary for the doping process.

Zinc oxide (ZnO) is a technologically very important semiconductor for the potential application in short wavelength light emitting devices.[1] This is due to its wide band gap (3.4 eV) and large exciton binding energy (60 meV). However, difficulties have been encountered in the control of the conduction type in this material. Up to now, the reproducible high quality *p*-type ZnO is still a challenge. It is expected that ion implantation might be an effective way to obtain the *p*-type ZnO. Efforts have been made to implant *p*-type dopants such as nitrogen and phosphorus into ZnO.[2–7] However, the implanted layer did not convert to *p*-type conductivity. The most probable origin is the implantation-induced defects, which may interfere with the activation of dopants or compensate the free carriers. The defects may also form stable complexes with the dopants and convert them into an electronically inactive state.[6] Therefore, detailed and systematic study of the thermal recovery of these defects is a very urgent task.

Positron annihilation spectroscopy[8] is a unique tool to study defects in semiconductors. The positron is particularly sensitive to vacancy-type defects, and shows clearly different annihilation behavior at vacancy sites as compared with the defect-free bulk state. Because of the missing atom, the electron density at the vacancy site is lowered, which leads to a longer positron lifetime. The possibility of positron annihilation with high momentum core electrons also decreases at the defect site, and then the Doppler broadening of positron annihilation radiation becomes narrower. In ZnO, Zn vacancies (V_{Zn}) have been identified by positrons in the as-grown bulk crystals and thin films[9–11] as well as electron irradiated samples.[12,13] Ion implantation produces more complicated defects because of the high density collision cascades, and vacancy clusters were then observed.[6,7,14]

It has been revealed that ZnO has high resistance to radiation damage.[15,16] This is due to the efficient dynamic annealing of the defects occurred during irradiation. For example, the vacancies produced by electron irradiation may easily recombine with the interstitials. Only those vacancy-interstitial pairs that are separated long distance can remain after irradiation.[15] However, recently an unusual behavior related to the implantation damage in ZnO was also observed. That is the chemical effect of the damage accumulation.[16] The implantation-induced defects can be stabilized by the implanted impurities and enhance damage buildup or even cause amorphization effects.[16]

In this work, we investigated the defects produced by B^+ and O^+ implantation by positron annihilation measurements

[a)]Electronic mail: chenzq@whu.edu.cn

using a slow positron beam. Raman scattering measurements were also conducted to acquire more information about the implantation-induced defects and their annealing process. Our results show clear difference in the defect recovery process for these two implanted specimens, which might be due to the chemical effects of the impurities. The possible mechanism for such chemical effects was tentatively discussed.

II. EXPERIMENT

The samples used in this work are hydrothermally grown ZnO single crystals from Scientific Production Company (SPC Goodwill). They are nominally undoped with *n*-type conductivity, and the carrier concentration is about 5.7×10^{12} cm^{-3}. Ion implantation was carried out at room temperature using a 400 keV implanter. A multistep implantation was performed for each ion with seven different energies. A box-shaped implantation profile with breadth of about 600 nm is then obtained after such implantation with appropriate dose for each energy. The energy range was 50–380 and 40–300 keV, and the total doses were 3.9×10^{15} and 5.2×10^{15} cm^{-2} for O^+ and B^+ implantation, respectively. After implantation, the samples were annealed isochronally from 200 to 1000 °C for 30 min in flowing nitrogen ambient.

A slow positron beam with energy variable from 0.2 to 30 keV was used for the positron annihilation study. Doppler broadening of positron annihilation radiation was measured as a function of incident positron energy using a high purity Ge detector. The *S* and *W* parameters defined as the ratio of the counts in the central region (511±0.77 keV) and wing region (511±3.4 to 511±6.8 keV) to the total area of the annihilation peak (511±8.5 keV) were used to characterize the measured spectrum. Micro-Raman-scattering measurements were performed using the Nanofinder spectrometer in the wave number range of 200–800 cm^{-1}. The 488.0 nm line of an Ar^+-ion laser was used for excitation and the incident laser power was ~1 mW. The spectral resolution is better than 4 cm^{-1}. The scattered light was detected in the backscattering geometry.

III. RESULTS AND DISCUSSION

In the as-grown sample, the conventional positron lifetime measurement reveals a single positron lifetime of about 182 ps, which is the bulk positron lifetime in ZnO we measured before.[10] Therefore, we believe that positrons are not trapped by vacancy defects in the as-grown sample, or the vacancy concentration is under the detection limit. Then the *S* parameters measured in this work were normalized to the bulk value in the as-grown sample. In this case, $S > 1$ reveals existence of vacancy defects which trap positrons.

Figure 1 shows the *S* parameter as a function of incident positron energy (*S*-*E* curve) for the as-grown and implanted samples by B^+ and O^+ ions. The higher *S* parameter at $E < 5$ keV is due to the positron diffusion and annihilation in the surface state. At $E > 7$ keV, the *S* parameter keeps at constant value in the as-grown sample, indicating positron annihilation in the bulk region of the sample. After ion implantation, an increase of the *S* parameter can be observed, which shows introduction of vacancy defects. The *S* parameter in the positron energy range of 5–13 keV is nearly constant, which corresponds to the box-shaped implantation layer, indicating a homogeneous distribution of vacancy defects. The *S* value of about 1.06 for O^+-implanted sample and 1.05 for B^+-implanted sample suggests that implantation produces mostly vacancy clusters, and the higher *S* parameter in the O^+-implanted sample implies a larger size or a higher concentration of vacancies. It should be noted that some small vacancies such as monovacancies may also have been introduced, which coexist with vacancy clusters.

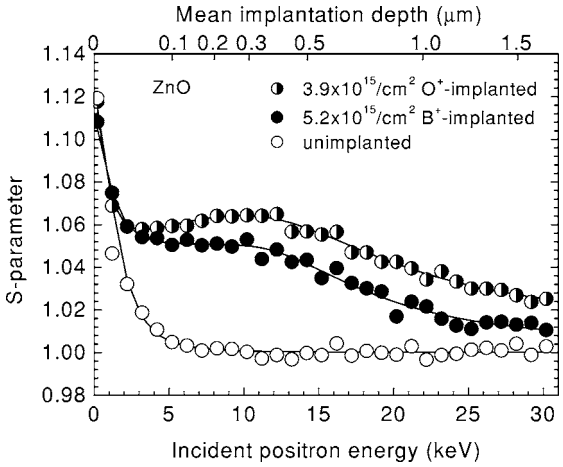

FIG. 1. *S*-*E* curves measured for ZnO samples before and after implantation. The solid lines are drawn as a guidance to the eye.

The most interesting result is the annealing process of the implantation-induced vacancies. Figure 2 shows some selected *S*-*E* curves measured for the O^+- and B^+-implanted

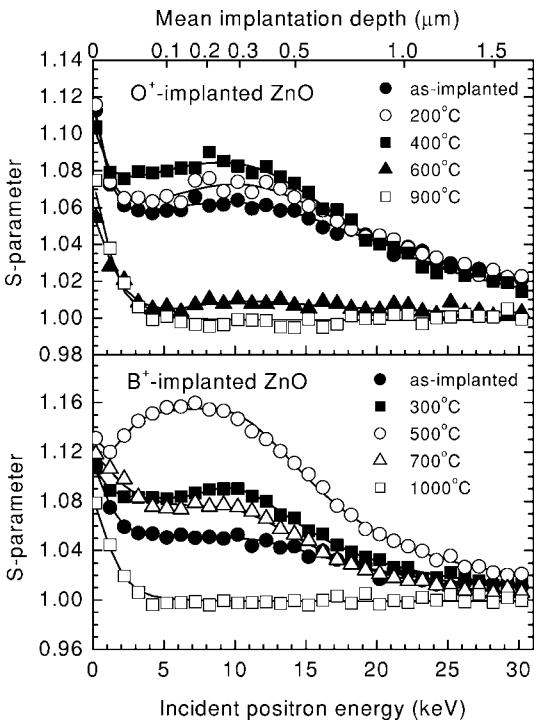

FIG. 2. *S*-*E* curves measured for O^+- and B^+-implanted ZnO samples after annealing. The solid lines are drawn as a guidance to the eye.

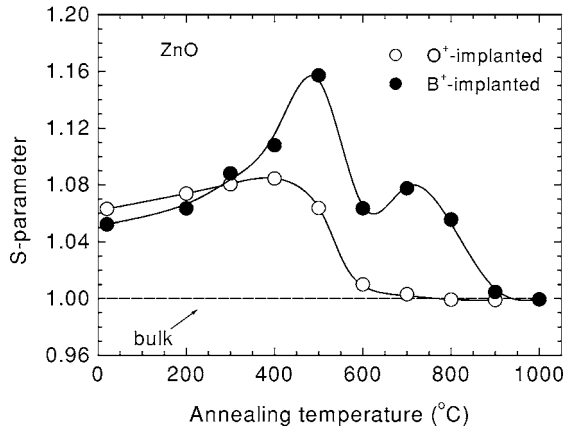

FIG. 3. Average *S* parameter in the implanted layer as a function of annealing temperature for the O^+- and B^+-implanted samples.

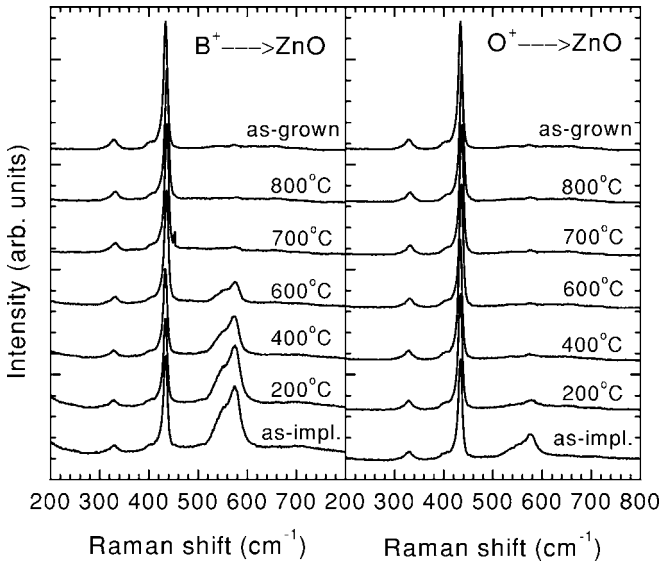

FIG. 4. Raman spectra measured for the O^+- and B^+-implanted ZnO samples after annealing.

samples after annealing. For each *S*-*E* curve, we summed the Doppler broadening spectra measured in the energy range of 5–9 keV, and obtained the average *S* parameter, which contains the defect information in the implanted box layer. The average *S* parameter as a function of annealing temperature is presented in Fig. 3. For the O^+-implanted ZnO, the *S* parameter first shows increase up to about 1.08 at 400 °C, and then decreases rapidly with increasing annealing temperature. Such increase of *S* parameter suggests mostly increase of the vacancy cluster size during annealing. This is due to the migration and agglomeration of vacancies. With increasing annealing temperature, the smaller vacancies such as monovacancies become mobile, and during their migration, they may encounter the vacancy clusters or other monovacancies to form larger vacancy clusters. This is an energetically favorable process. After further annealing at high temperatures, these vacancy clusters are no longer stable, and they gradually recover. At 700–800 °C, the *S* parameter decreases to the bulk value, suggesting full recovery of these vacancies.

For the B^+-implanted sample, the annealing behavior of the vacancies is similar. However, the *S* parameter increases to a high value of nearly 1.16 after annealing at 500 °C. This means that much larger vacancy clusters or microvoids are formed through annealing. After annealing at 600 °C, the *S* parameter begins to decrease. However, it shows a small increase again at 700 °C, and after that, it decreases gradually to the bulk value at 900–1000 °C, which indicates annealing out of the vacancy defects introduced by implantation. The increase of *S* parameter at 700 °C is repeatable by performing the same annealing process on another B^+-implanted ZnO film sample grown by pulsed laser deposition. Nevertheless, the underlying mechanism for such abnormal increase is not fully understood at present.

The TRIM (Ref. 17) simulation shows that the average vacancy concentration produced by O^+ implantation in the box layer is about 7×10^{22} cm^{-3}, while it is 4×10^{22} cm^{-3} for B^+ implantation. Therefore, it is expected that a little larger size or higher concentration of vacancy clusters will be formed in the O^+-implanted sample. This has been reflected by a higher *S* parameter in the O^+ as-implanted ZnO. Nevertheless, after annealing, the *S* parameter shows very slight increase in this sample, suggesting that further agglomeration of the vacancy clusters is very weak. On the contrary, for the B^+-implanted sample, the vacancy clusters grow into very large size through agglomeration during annealing process. This suggests that boron might have a special chemical effect that favors the agglomeration of vacancy clusters. We have observed the similar chemical effect in the Al^+-implanted ZnO. From the comparison of the Al^+ and P^+ implantation with the same implantation condition, we found different annealing behaviors for the implantation-induced defects. The vacancies in the Al^+-implanted sample agglomerated into microvoids after annealing, which was indicated by a much higher *S* parameter of 1.25 at 600 °C. While for P^+-implanted sample, the *S* parameter increased only to a maximum value of 1.15 after annealing at 600 °C.[7]

Figure 4 shows the Raman spectra measured for the O^+- and B^+-implanted samples before and after annealing. In the as-grown ZnO, there are three phonon modes: E_2 at 437 cm^{-1}, A_1 (LO) at 575 cm^{-1}, and a multiphonon mode at 331 cm^{-1}. These modes have been commonly observed and discussed in detail by others.[18,19] The other Raman active phonon modes such as E_1 (LO), E_1 (TO), and A_1 (TO) expected from the group theory are not seen in our measurement because of the backscattering geometry. The dominant peak E_2 is characteristic of the ZnO wurtzite structure and the peak at 575 cm^{-1} might be induced by defects. After implantation, the peak at 575 cm^{-1} becomes strong and broad. This is apparently due to the implantation-induced damage, which has been observed in other ion-implanted ZnO.[3,7,20] The high density of defects introduced by implantation cut the long range lattice ordering, therefore the Raman selection rules are relaxed, and many other phonon modes which are forbidden in the perfect lattice participate in the Raman spectrum, thus contribute to the broad peak at 575 cm^{-1}. This broad peak has been attributed to the oxygen vacancy (V_O) since it also appears in the ZnO grown under oxygen deficient condition.[21,22] In the electron irradiated

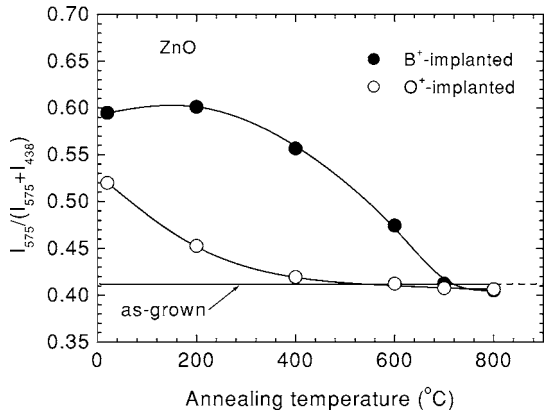

FIG. 5. Relative ratio of the integrated 575 cm^{-1} peak intensity to the sum of the 437 and 575 cm^{-1} peaks as a function of annealing temperature for the O^+- and B^+-implanted ZnO.

ZnO, we also observed the same Raman peak at around 575 cm^{-1},[23] and the thermal recovery of this broad peak agreed well with that of oxygen vacancies.[24]

From Fig. 4, we can see that the broad peak in the O^+-implanted sample is much smaller than that in the B^+-implanted one, which implies a much lower concentration of oxygen vacancies produced by O^+ implantation. This result also supports the assignment of the broad peak at 575 cm^{-1} to V_O induced phonon mode. Much of the V_O will be killed by the implanted O^+, which results in a relatively lower concentration of V_O. As the V_O is invisible to positrons,[10,13] Raman scattering measurements give us complimentary information about defect evolution during annealing process.

With increasing annealing temperature, the broad peak in both O^+- and B^+-implanted samples decreases gradually. However, their annealing processes show some differences. We integrated the intensity of the broad defect peak (500–640 cm^{-1}) and calculate its ratio to the sum of the 575 and 437 cm^{-1} peak (380–640 cm^{-1}). This ratio is plotted in Fig. 5 as a function of the annealing temperature. In the O^+-implanted sample, the 575 cm^{-1} peak decreases rapidly and reaches the same level as the unimplanted sample after annealing at 400 °C. This means that V_O disappears early at 400 °C. While for the B^+-implanted sample, the broad peak remains high intensity until annealing at 700 °C, indicating that V_O has much higher thermal stability in the B^+-implanted ZnO.

We may find the correlation between the Raman data and the positron annihilation results. Agglomeration of vacancy clusters involves combining small vacancies such as monovacancies (V_{Zn} and V_O), so that the size of vacancy cluster increases. This means that V_O has a contribution to the vacancy cluster agglomeration. In the O^+-implanted sample, the number of V_O is much smaller as compared with that in the B^+-implanted sample, and they disappear rapidly after annealing, therefore their contribution to the vacancy cluster growth is also small. In other words, the agglomeration of vacancy clusters is limited due to the low concentration and weak thermal stability of V_O. This might be the reason for the slight increase of S parameter after annealing. When V_O disappears at 400 °C, the agglomeration of vacancy clusters also comes to a stop. For the B^+-implanted sample, it introduces much higher concentration of V_O, and they are stable up to 700 °C, thus the vacancy cluster can grow into a sufficiently large size. This may well explain the positron annihilation results.

The chemical effect of boron is thus due to the stabilization of V_O. During annealing, the oxygen vacancies may recover mainly in two ways: one is the recombination with oxygen interstitials (O_i), another way is the migration to sinks. The boron impurity might trap O_i produced by implantation and form oxide complexes such as B_2O_3. Since the B_2O_3 compound has a much lower enthalpy of formation (−1273.5 kJ/mol) than ZnO (−350.5 kJ/mol),[25] the formation of such complex is very likely. Due to this complex formation, the recombination of V_O with O_i is suppressed, so the oxygen vacancies are stabilized. When these mobile oxygen vacancies cannot find sinks to anneal, they are likely to contribute to the formation of large vacancy clusters or microvoids through agglomeration. While for O^+ implantation, as it is a self-atom in ZnO, there is no complex formation with O_i. On the contrary, the O^+ implantation produces large amounts of oxygen interstitials, which will expedite the recombination of V_O with them. Therefore, we can observe a fast recovery process of the oxygen vacancies. The agglomeration of the vacancy clusters is therefore suppressed.

The analysis of the *S-W* plot from the Doppler broadening measurements shown above can give some information about the defect complexes involving the implanted impurities. However, the *S-W* plot for the O^+- and B^+-implanted samples shows nothing special. This means that the implanted O^+ and B^+ do not form complexes with the vacancy defects. The implanted oxygen atoms are probably activated from interstitial site to the ZnO lattice location after annealing, while most of the B impurities are combined with the O_i as suggested by the Raman measurements.

In our previously Al^+-implanted sample, the Al_2O_3 complexes may also have been formed, which has been suggested by many other researchers,[26,27] as it has even lower enthalpy of formation (−1675.7 kJ/mol) than that of B_2O_3. Therefore a very high Doppler broadening S parameter was observed after annealing at 600 °C, which suggests formation of large amounts of microvoids.[14] Similar chemical effect of the damage accumulation has also been observed in other materials, for example, the C^+-implanted Si (Refs. 28 and 29) and GaN.[30] The SiC complex formation was proposed to explain the chemical effects in C^+-implanted Si.[28]

IV. CONCLUSION

Positron annihilation and Raman measurements for the B^+- and O^+-implanted ZnO show that the annealing process of the implantation-induced vacancy defects depends on the ion species. The boron impurities might trap oxygen interstitials and form complexes, which stabilize the oxygen vacancies up to 700 °C. These oxygen vacancies are coalesced with vacancy clusters and evolve into microvoids. A high annealing temperature of 900–1000 °C is needed to fully remove these microvoids. On the contrary, the oxygen vacancies in the O^+-implanted sample are easily removed at low

annealing temperature of 400 °C. As a result, the vacancy agglomeration process is limited and no microvoid is observed. A lower temperature of 700–800 °C is enough to anneal out all the vacancy defects in this sample.

[1] S. J. Pearton, D. P. Norton, K. Ip, Y. W. Heo, and T. Steiner, Prog. Mater. Sci. **90**, 293 (2005).
[2] B. W. Thomas and D. Walsh, J. Phys. D **6**, 612 (1973).
[3] F. Reuss, C. Kirchner, Th. Gruber, R. Kling, S. Maschek, W. Limmer, A. Waag, and P. Ziemann, J. Appl. Phys. **95**, 3385 (2004).
[4] C.-C. Lin, S.-Y. Chen, and S.-Y. Cheng, Appl. Surf. Sci. **238**, 405 (2004).
[5] G. Xiong, K. B. Ucer, R. T. Williams, J. Lee, D. Bhattacharyya, J. Metson, and P. Evans, J. Appl. Phys. **97**, 043528 (2005).
[6] Z. Q. Chen, M. Maekawa, A. Kawasuso, R. Suzuki, and T. Ohdaira, Appl. Phys. Lett. **87**, 091910 (2005).
[7] Z. Q. Chen, A. Kawasuso, Y. Xu, H. Naramoto, X. L. Yuan, T. Sekiguchi, R. Suzuki, and T. Ohdaira, J. Appl. Phys. **97**, 013528 (2005).
[8] R. Krause-Rehberg and H. S. Leipner, *Positron Annihilation in Semiconductors, Defect Studies*, Springer Series in Solid-State Sciences, Vol. 127 (Springer, Berlin, 1999).
[9] A. Uedono, T. Koida, A. Tsukazaki, M. Kawasaki, Z. Q. Chen, S. F. Chichibu, and H. Koinuma, J. Appl. Phys. **93**, 2481 (2003).
[10] Z. Q. Chen, S. Yamamoto, M. Maekawa, A. Kawasuso, X. L. Yuan, and T. Sekiguchi, J. Appl. Phys. **94**, 4807 (2003).
[11] A. Zubiaga, F. Tuomisto, F. Plazaola, K. Saarinen, J. A. Garcia, J. F. Rommeluere, J. Zuniga-Perez, and V. Munoz-Sanjose, Appl. Phys. Lett. **86**, 042103 (2005).
[12] S. Brunner, W. Puff, A. G. Balogh, and P. Mascher, Mater. Sci. Forum **363–365**, 141 (2001).
[13] F. Tuomisto, V. Ranki, K. Saarinen, and D. C. Look, Phys. Rev. Lett. **91**, 205502 (2003).
[14] Z. Q. Chen, M. Maekawa, S. Yamamoto, A. Kawasuso, X. L. Yuan, T. Sekiguchi, R. Suzuki, and T. Ohdaira, Phys. Rev. B **69**, 035210 (2004).
[15] D. C. Look, D. C. Reynolds, C. W. Litton, R. L. Jones, D. B. Eason, and G. Cantwell, Appl. Phys. Lett. **81**, 1830 (2002).
[16] S. O. Kucheyev, J. S. Williams, C. Jagadish, J. Zou, C. Evans, A. J. Nelson, and A. V. Hamza, Phys. Rev. B **67**, 094115 (2003).
[17] J. P. Biersack and L. G. Haggmark, Nucl. Instrum. Methods **174**, 257 (1980).
[18] T. C. Damen, S. P. S. Porto, and B. Tell, Phys. Rev. **142**, 570 (1966).
[19] J. M. Calleja and M. Cardona, Phys. Rev. B **16**, 3753 (1977).
[20] T. S. Jeong, M. S. Han, C. J. Youn, and Y. S. Park, J. Appl. Phys. **96**, 175 (2004).
[21] J. N. Zeng, J. K. Low, Z. M. Ren, T. Liew, and Y. F. Lu, Appl. Surf. Sci. **197**, 362 (2002).
[22] C. J. Youn, T. S. Jeong, M. S. Han, and J. H. Kim, J. Cryst. Growth **261**, 526 (2004).
[23] Z. Q. Chen, M. Maekawa, A. Kawasuso, S. Sakai, and H. Naramoto, Physica B **376–377**, 722 (2006).
[24] L. S. Vlasenko and G. D. Watkins, Phys. Rev. B **71**, 125210 (2005).
[25] *CRC Handbook of Chemistry and Physics*, 81st ed., edited by D. R. Lide (CRC, Boca Raton, FL, 2000).
[26] C. Agashe, O. Kluth, J. Hupkes, U. Zastrow, B. Rech, and M. Wutting, J. Appl. Phys. **95**, 1911 (2004).
[27] K.-K. Kim, S. Niki, J.-Y. Oh, J.-O. Song, T.-Y. Seong, S.-J. Park, S. Fujita, and S.-W. Kim, J. Appl. Phys. **97**, 066103 (2005).
[28] J. P. de Souza, H. Boudinov, and P. F. P. Fichtner, Appl. Phys. Lett. **64**, 3596 (1994).
[29] J. P. de Souza, Yu. Suprun-Belevich, H. Boudinov, and C. A. Cima, J. Appl. Phys. **87**, 8385 (2000).
[30] S. O. Kucheyev, J. S. Williams, C. Jagadish, J. Zou, G. Li, and A. I. Titov, Phys. Rev. B **64**, 035202 (2001).